toxics

MDPI

Article

Effects of Potassium Iodide on Proliferation of RET/PTC1-Rearranged TPC-1 Cells and Their Association with PI3K/AKT/mTOR Signaling

Siyu Liu [1,2], Xiaomeng Yu [2], Peisen Ding [2,3], Zhilei Xing [2], Yushan Cui [1,*] and Hongliang Liu [2,*]

[1] Institute of Environment and Health, Tianjin Centers for Disease Control and Prevention, 6 Huayue Road, Hedong District, Tianjin 300011, China
[2] Department of Epidemiology and Health Statistics, School of Public Health, Tianjin Medical University, 22 Qixiangtai Road, Heping District, Tianjin 300070, China
[3] Department of Science and Education, Tianjin First Central Hospital, Tianjin 300192, China
* Correspondence: yushan.273@163.com (Y.C.); hongliang_liu@sina.com (H.L.)

Abstract

We examined potassium iodide (KI)-associated responses in RET/PTC1-rearranged TPC-1 cells. Cells were exposed to 10^{-6}–10 mmol/L KI for 12, 24, or 48 h; CCK-8, EdU incorporation, wound-healing, flow-cytometric, and immunoblot assays assessed relative metabolic viability, DNA synthesis, wound closure, cell cycle distribution, and protein signals. KI responses varied with concentration and time. At 48 h, the CCK-8 signal was highest in the 10^{-3} mmol/L group (129.57 ± 1.67% of control) and lower in the 10 mmol/L group. At 10^{-3} mmol/L, KI was associated with increased EdU positivity, wound closure, S-phase fraction, proliferation index, and Cyclin D1, together with reduced PTEN and higher p-AKT/AKT and p-P70S6K/P70S6K ratios; the p-mTOR/mTOR ratio was not significantly increased. LY294002 (10 μmol/L) was combined with 10^{-3} mmol/L KI for 48 h. Relative to KI alone, combined LY294002 and KI treatment was associated with lower EdU positivity, wound closure, S-phase fraction, proliferation index, Cyclin D1, and phospho-to-total AKT, mTOR, and P70S6K ratios, and a higher G_0/G_1 fraction and PTEN signal. In this RET/PTC1-rearranged cell model, these observations are consistent with involvement of PI3K/AKT/mTOR-related signaling in KI-associated responses.

Keywords: papillary thyroid carcinoma; potassium iodide; RET/PTC1 rearrangement; PI3K/AKT/mTOR signaling pathway; cell cycle

Check for updates

Academic Editor: Francesca Gorini

Received: 28 October 2026
Revised: 18 November 2026
Accepted: 26 November 2026
Published: 28 November 2026

Copyright: © 2026 by the authors. Licensee MDPI, Basel, Switzerland. This article is an open access article distributed under the terms and conditions of the Creative Commons Attribution (CC BY) license.

1. Introduction

In 2020, an estimated 586,000 new cases of thyroid cancer were reported worldwide, accounting for 3.0% of all new cancer cases; thyroid cancer accounted for approximately 0.4% of cancer deaths [1]. Chinese cancer statistics for 2022 ranked thyroid cancer third among newly diagnosed malignancies [2], and its burden among adolescents and young adults also warrants attention [3]. Differentiated thyroid cancers include papillary thyroid carcinoma (PTC), follicular thyroid carcinoma, and oncocytic thyroid carcinoma; PTC is the most common histological type [4,5]. The rising incidence of thyroid cancer is associated with advances in diagnostic technologies and overdiagnosis, while the contribution of environmental exposures has also attracted attention [6].

Iodine is an essential micronutrient for thyroid hormone synthesis, and its health effects depend on intake, exposure source, and individual susceptibility. In addition to dietary

sources, drinking water, supplements, and iodine-containing preparations may affect iodine burden [7,8]. Previous studies have used different iodine exposure measures, populations, and experimental models, and their findings have not been fully consistent [9,10]. A systematic review and meta-analysis suggested a possible positive association between high iodine exposure and PTC risk [11]. An updated meta-analysis published in 2026 further reported associations of higher urinary iodine concentrations with increased risks of thyroid cancer, PTC, and papillary thyroid microcarcinoma, whereas the association between dietary iodine intake and thyroid cancer risk remained unclear [12]. Iodine concentrations in groundwater and drinking water vary substantially by geography, and some regions continue to face water-borne iodine excess [13–18]. Studying thyroid cell responses under defined iodine exposure forms and concentrations may therefore help clarify biological processes underlying population-level associations.

The PI3K/AKT/mTOR pathway participates in cell survival, proliferation, and cell cycle regulation, and its dysregulation is associated with thyroid cancer progression [19,20]. In vitro studies have reported that high iodine can increase AKT phosphorylation in thyroid cancer cells and promote proliferation through AKT/Wee1/CDK1-related regulation [21]. Other work has shown effects of high iodine on proliferation, apoptosis, migration, and autophagy in BRAF-mutant PTC cells [22]. PTC arises in distinct molecular-driver contexts, including RET fusions [23]. TPC-1 cells harbor a RET/PTC1 (CCDC6–RET) rearrangement and provide a model for studying signaling responses in this molecular context [24]. Integrating KI exposure with cellular phenotypes and related signaling changes can provide experimental evidence on the effects of iodine in RET/PTC1-rearranged PTC cells.

Here, we used RET/PTC1-rearranged TPC-1 cells and potassium iodide (KI) as the form of iodine exposure. RET/PTC fusions can constitutively engage MAPK signaling, contributing to loss of thyroid differentiation and reduced expression of proteins involved in iodide handling and thyroid hormone synthesis. Loss of functional iodide uptake can limit radioiodine treatment efficacy [25]. This clinical context should be distinguished from the response to KI added to cultured TPC-1 cells. Genetic and functional studies have characterized TPC-1 as a RET/PTC1-bearing model with features distinct from BRAF-mutant PTC cells [26,27].

We screened cell-viability responses across a broad concentration range and examined EdU incorporation, wound closure, cell cycle distribution, and PTEN, PI3K/AKT/mTOR/P70S6K, and Cyclin D1 protein signals. LY294002 was then used as a pharmacological intervention to explore the involvement of PI3K/AKT/mTOR-related signaling in the cellular response to KI.

2. Materials and Methods

2.1. Reagents

The PI3K inhibitor LY294002 (MCE, Monmouth Junction, NJ, USA, CAS No. 154447-36-6; purity > 99.9%) was dissolved in DMSO with sonication to prepare a 20 mmol/L stock solution and diluted in culture medium to the required concentrations. The final DMSO concentration was 0.05% (v/v) in the Ctrl, KI, and LY+KI groups of the intervention experiments. Potassium iodide (KI; Aladdin, Shanghai, China, P433794; analytical-grade) was prepared in sterile solvent and added to culture medium at the indicated concentrations. KI working solutions were freshly prepared and protected from light during preparation and handling. The cell cycle and apoptosis analysis kit was obtained from Beyotime Biotechnology (C1052, Shanghai, China), and DMSO was purchased from Solarbio (D8371, Beijing, China). LY294002 was used as a pharmacological inhibitor of PI3K signaling [28–30].

2.2. Cell Line and Culture

The human PTC cell line TPC-1 was obtained from Procell Life Science & Technology Co., Ltd. (Wuhan, China; CL-0643). Cells were cultured in complete RPMI 1640 medium containing 10% fetal bovine serum and 1% penicillin–streptomycin solution at 37 °C in a humidified incubator with 5% CO_2. Cells at passages below 5 were used for the experiments.

2.3. Exposure Design and Groups

For the KI concentration screen, cells were treated with 0, 10^{-6}, 10^{-5}, 10^{-4}, 10^{-3}, 10^{-2}, 10^{-1}, 1, or 10 mmol/L KI for 12, 24, or 48 h. KI exposure in subsequent experiments lasted 48 h. EdU assays compared the control with 10^{-5}, 10^{-3}, 10^{-1}, and 10 mmol/L KI. Concentration-response analyses of pathway proteins and the cell cycle included the control and 10^{-5}, 10^{-3}, and 10^{-1} mmol/L KI groups. For intervention experiments, cells received vehicle (Ctrl), 10^{-3} mmol/L KI (KI), or 10 μmol/L LY294002 plus 10^{-3} mmol/L KI (LY+KI); LY294002 and KI were added simultaneously. The 10^{-3} mmol/L KI concentration was selected for intervention experiments because it produced the highest mean CCK-8 signal at 48 h and increased EdU positivity in the initial screen. A preliminary 48 h single-agent concentration screen identified 10 μmol/L LY294002 for subsequent intervention. For 48 h exposures, the culture medium was replaced after 24 h with fresh medium of the same volume containing KI and, where applicable, LY294002 at the original treatment concentrations.

2.4. CCK-8 and EdU Assays

The CCK-8 kit was purchased from Solarbio (Beijing, China; CA1210). TPC-1 cells were seeded in 96-well plates at 3000 cells in 90 μL of cell suspension per well and allowed to attach for 4 h at 37 °C with 5% CO_2. Subsequently, 10 μL of the appropriate KI working solution was added to each well to obtain the indicated final concentration in a treatment volume of 100 μL. At each assay endpoint, 10 μL of CCK-8 reagent was added per well, followed by incubation for 4 h at 37 °C with 5% CO_2. Absorbance was read at 450 nm using a K-LAB MRX-A2000 microplate reader (K-LAB, Shanghai, China). Blank wells contained medium and CCK-8 reagent without cells, and blank absorbance was subtracted before calculation. Values were normalized to the corresponding control at each time point and are reported as relative cell viability. Six technical wells were used per group in each independent experiment. The EdU assay kit was purchased from Beyotime Biotechnology (Shanghai, China; C0071S). Logarithmically growing cells were seeded on coverslips in 12-well plates at 1×10^4 cells in 1 mL of treatment medium per well, with KI added at seeding. After treatment, cells were labeled with 10 μmol/L EdU for 2 h and processed according to the manufacturer's instructions. Total nuclei were counterstained with Hoechst 33342. Images were acquired using an Olympus IX81 microscope (Olympus, Tokyo, Japan) with a 10× objective and cellSens Dimension 1.18, and analyzed using ImageJ 1.53k. Five fields were analyzed per well, with at least 500 nuclei counted. EdU-positive and total nuclei were pooled across fields within each well, and DNA synthesis was expressed as the percentage of EdU-positive nuclei among total nuclei.

2.5. Wound Healing Assay

Three parallel lines at defined intervals were drawn on the underside of each 6-well plate. TPC-1 cells were seeded at 6×10^5 cells per well in 2 mL of cell suspension and cultured to form an attached monolayer. A scratch perpendicular to the marked lines was made with a 200-μL pipette tip using consistent pressure. Cells were washed three times with PBS and cultured in 2 mL of medium containing 0.5% FBS with the indicated treatments. The low-serum condition was used to reduce serum-stimulated proliferation during wound closure. Five fields per well were imaged at the same positions at 0 and

48 h using an Olympus IX81 microscope (Olympus, Tokyo, Japan) with a 10× objective and cellSens Dimension 1.18. Wound area was measured using ImageJ 1.53k. Wound closure was calculated as $(A_0 - A_{48})/A_0 \times 100\%$, where A_0 and A_{48} denote the wound areas at 0 and 48 h, respectively.

2.6. Cell Cycle Analysis

The cell cycle and apoptosis analysis kit was purchased from Beyotime Biotechnology (Shanghai, China; C1052). Approximately 1×10^6 cells were prepared per sample using T25 culture flasks containing 5 mL of medium with the indicated treatments for 48 h. Cells were harvested, washed with cold PBS, fixed in ice-cold 70% ethanol at 4 °C for at least 30 min, and washed again with PBS. Each sample was resuspended in 0.5 mL of propidium iodide/RNase A staining solution and incubated at 37 °C for 30 min in the dark, according to the manufacturer's instructions. Cell cycle distribution (G_0/G_1, S, and G_2/M phases) was measured using a CytoFLEX SRT flow cytometer (Beckman Coulter, Brea, CA, USA) and analyzed using the univariate cell cycle platform in FlowJo 10.8.1. Approximately 30,000–50,000 events were acquired per sample at a low flow rate. Intact cells were selected using FSC-A/SSC-A, and doublets and aggregates were excluded using DNA-fluorescence pulse parameters (PE-A/PE-W). DNA fluorescence (PE-A) was analyzed on a linear scale, with sub-G1 events excluded from the G_0/G_1, S, and G_2/M fit. The phase values exported from the cell cycle analysis were used to calculate the S-phase fraction (SPF) and proliferation index (PI) with a common sum-of-phases denominator, as follows: $SPF = S/(G_0/G_1 + S + G_2/M) \times 100\%$; $PI = (S + G_2/M)/(G_0/G_1 + S + G_2/M) \times 100\%$.

2.7. Western Blotting

Cells were cultured in T25 flasks (25 cm^2) containing 5 mL of medium and lysed on ice at approximately 4 °C using strong RIPA lysis buffer (Servicebio, Wuhan, China; G2002-100ML) supplemented with 50× protease inhibitor cocktail (Servicebio, Wuhan, China; G2006-250UL; 1:50), phosphatase inhibitor (Servicebio, Wuhan, China; G2007-1ML; 1:50), and PMSF at a final concentration of 1 mmol/L. The buffer was added at approximately 50–100 µL per 1×10^6 cells (approximately 150–250 µL per well of a 6-well plate). After 3–5 min of contact with the buffer, cells were scraped into 1.5-mL tubes and kept on ice for another 2–10 min, with repeated pipetting to complete lysis. Samples were subjected to two centrifugation steps, each at approximately 9700 × *g* for 20 min at 4 °C using an Allegra C-34R centrifuge with a CF 12.2 fixed-angle rotor (Beckman Coulter, Brea, CA, USA), and sonicated for 30 s during protein extraction. Supernatants were collected for protein analysis. Protein concentrations were measured using a BCA protein assay kit (Solarbio, Beijing, China; PC0020) and equalized before electrophoresis. Proteins were separated by SDS-PAGE and transferred to PVDF membranes. Membranes were blocked for 1 h at room temperature using protein-free rapid blocking buffer (YamayBio/Epizyme, Shanghai, China; PS108) and incubated overnight at 4 °C with primary antibodies. All primary antibodies were from Cell Signaling Technology (CST, Danvers, MA, USA): PI3K p110α (#4249; 1:1000), phospho-PI3K p85 Tyr458/p55 Tyr199 (#4228; 1:1000), PTEN (#9559; 1:1000), AKT (#4691; 1:1000), phospho-AKT Ser473 (#4060; 1:2000), mTOR (#2983; 1:1000), phospho-mTOR Ser2448 (#5536; 1:1000), P70S6K (#34475; 1:1000), phospho-P70S6K Thr389 (#97596; 1:1000), Cyclin D1 (#55506; 1:1000), GAPDH (#2118; 1:1000), and β-actin (#4970; 1:1000). Primary antibodies were diluted in universal antibody diluent (YamayBio/Epizyme; PS119L). Membranes were incubated with HRP-conjugated goat anti-rabbit IgG H&L secondary antibody (Abcam, Cambridge, UK; ab6721; 1:10,000) for 1 h and washed with TBST containing 0.05% Tween 20. Bands were developed using the Super Excellent Chemiluminescent Substrate (ECL) Detection Kit (Elabscience, Wuhan, China; E-IR-R308), and imaged

using a ChemiDoc XRS+ system (Bio-Rad, Hercules, CA, USA). Image Lab 6.1 was used for image acquisition and densitometry. Densitometry was performed without background subtraction, using nonsaturated bands within the verified linear detection range. Signals were normalized to GAPDH or β-actin, as appropriate for each membrane, and expressed relative to the control. Phosphorylated and corresponding total protein measurements were paired within each independent experiment to calculate p-AKT/AKT, p-mTOR/mTOR, and p-P70S6K/P70S6K ratios. The approximately 85 kDa phospho-antibody-reactive signal and the p110α signal represent different PI3K subunits. Their quotient is presented only as a cross-subunit signal ratio, not as the fraction of PI3K phosphorylated. The KI concentration and LY294002 intervention immunoblots were obtained in separate experimental batches, each with its own controls.

2.8. Statistical Analysis

Each experiment was independently repeated three times ($n = 3$). Measurements from image fields were first pooled within each well, and technical replicates were then averaged to obtain one group-level value per independent experiment for statistical analysis. CCK-8 used six technical wells per group per independent experiment; three technical replicates were used for the other assays. Data are presented as mean ± standard deviation. Two-group comparisons were performed using independent-samples *t* tests. Multiple groups were compared using a one-way analysis of variance followed by Tukey's multiple-comparisons test using SPSS 24.0. KI concentration-response cell cycle data were analyzed in GraphPad Prism 11.0. Cell cycle distribution was analyzed using an ordinary two-way analysis of variance with KI concentration and phase as factors, followed by Tukey's multiple comparisons within each phase. SPF and PI were analyzed by an ordinary two-way analysis of variance with KI concentration and index type as factors, followed by Šídák's multiple comparisons within each index. The cross-subunit PI3K signal ratio and matched phospho-to-total ratios were analyzed in Prism 11.0 using ordinary two-way ANOVA with treatment and ratio type as factors, followed by Dunnett's control comparisons for the KI concentration experiment and Tukey's comparisons for the intervention experiment. For the LY294002 intervention cell cycle experiment, SPF and PI were analyzed by a two-way repeated-measures ANOVA, matching both factors, followed by Šídák's comparisons within each index. The phase distribution was assessed by an ordinary two-way ANOVA followed by Tukey's comparisons within each phase. Adjusted *p* values are reported for multiple comparisons. $p < 0.05$ was considered statistically significant.

3. Results

3.1. Effects of KI Exposure on TPC-1 Cell Growth and Proliferation

CCK-8 signals varied with KI concentration and exposure time (Table 1 and Figure 1A). At 12 h, the 10 mmol/L group was lower than the control ($p < 0.05$). At 24 h, the 10^{-5}, 10^{-3}, and 10^{-2} mmol/L groups were higher than the control (all $p < 0.05$). At 48 h, viability increased in the 10^{-5}, 10^{-3}, and 10^{-1} mmol/L groups and decreased in the 10 mmol/L group (all $p < 0.05$). The 10^{-3} mmol/L group had a relative cell viability of 129.57 ± 1.67%, the highest mean among the concentrations tested at this time point. These findings indicate that the KI effect did not increase continuously with concentration.

The CCK-8 assay provided a metabolic viability readout, and EdU incorporation was used to assess DNA synthesis. EdU analysis showed higher proportions of EdU-positive cells after 48 h of treatment with 10^{-5} and 10^{-3} mmol/L KI than in the control (both $p < 0.05$; Figure 1B,C), consistent with the increased viability signal. Wound-healing analysis was then performed with 10^{-3} mmol/L KI. The wound closure at 48 h was higher in this group than in the control ($p < 0.01$; Figure 1D,E), indicating increased wound closure.

Table 1. Relative cell viability of TPC-1 cells after treatment with different KI concentrations (%). Values are mean ± standard deviation ($n = 3$).

KI (mmol/L)	12 h	24 h	48 h
0	100.44 ± 1.31	100.32 ± 1.88	100.76 ± 0.88
10^{-6}	103.95 ± 4.37	99.61 ± 10.77	107.82 ± 3.36
10^{-5}	107.83 ± 8.60	117.10 ± 7.97 *	118.60 ± 1.96 *
10^{-4}	104.65 ± 8.98	113.63 ± 9.86	111.60 ± 6.33
10^{-3}	105.42 ± 6.82	117.99 ± 6.74 *	129.57 ± 1.67 *
10^{-2}	100.86 ± 13.75	117.24 ± 6.09 *	110.52 ± 1.76
10^{-1}	94.21 ± 8.85	109.71 ± 12.91	123.04 ± 3.06 *
1	91.53 ± 16.44	104.14 ± 11.82	94.34 ± 8.04
10	86.45 ± 15.92 *	100.51 ± 16.82	83.72 ± 2.43 *

* $p < 0.05$ compared with 0 mmol/L KI at the same time point.

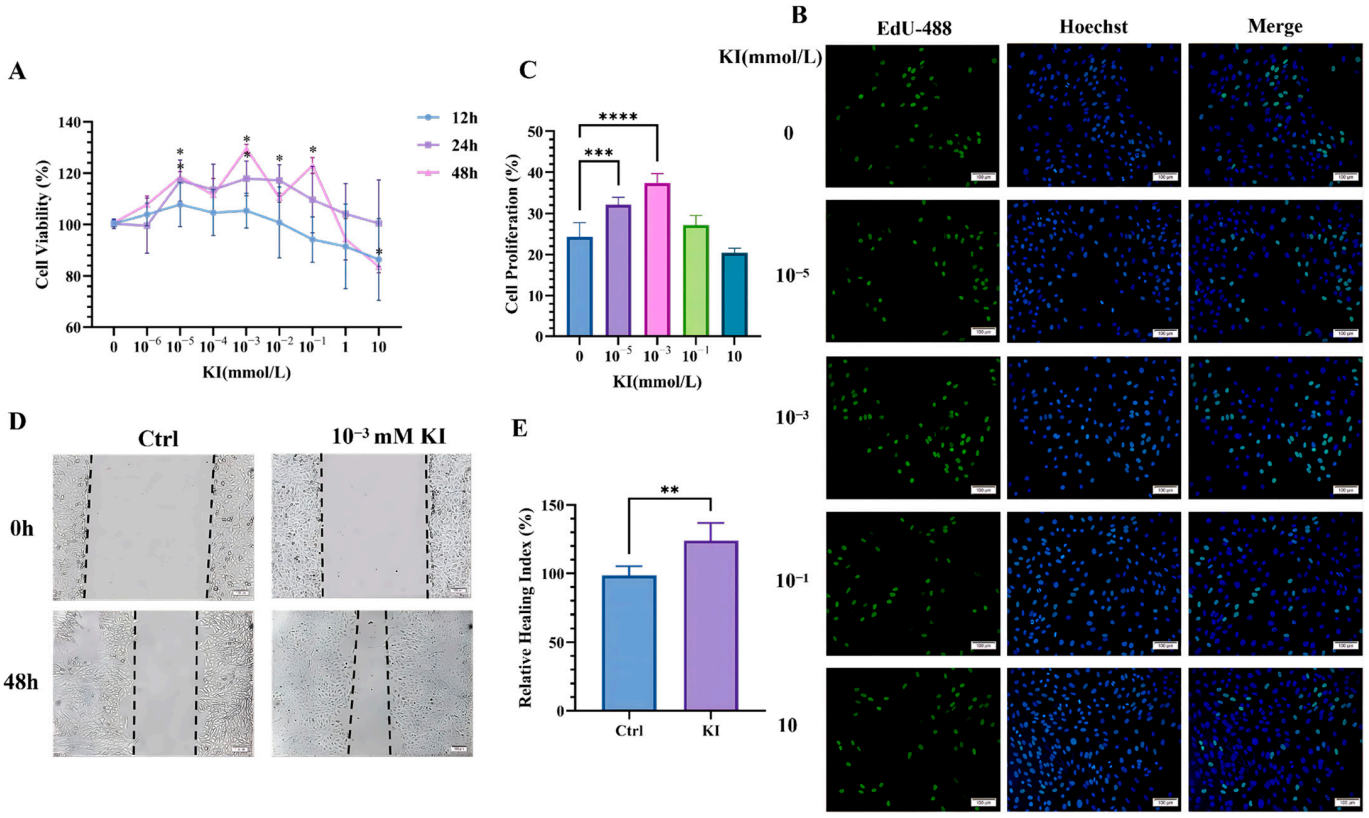


Figure 1. Effects of KI exposure on TPC-1 cell viability, DNA synthesis, and wound closure. (**A**) CCK-8 results after treatment with the indicated KI concentrations for 12, 24, or 48 h; data are mean ± SD. (**B**) Representative EdU images after 48 h of treatment with vehicle or 10^{-5}, 10^{-3}, 10^{-1}, or 10 mmol/L KI; scale bar, 100 µm. (**C**) Percentage of EdU-positive cells, shown as bar plots representing mean ± SD. (**D**) Representative wound images at 0 and 48 h for control and 10^{-3} mmol/L KI groups; scale bar, 100 µm. (**E**) Wound closure at 48 h; data are mean ± SD. Each experiment was independently repeated three times ($n = 3$). Panels (**A**), analyzed separately at each time point, and (**C**) were assessed by a one-way ANOVA with Tukey's multiple-comparisons test; panel (**E**) was assessed by an independent-samples *t* test. Asterisks in (**A**,**C**) indicate comparisons with the control at the same time point or the corresponding control group; brackets in (**E**) indicate the groups compared. * $p < 0.05$; ** $p < 0.01$. In (**A**), blue, purple, and pink lines indicate 12, 24, and 48 h, respectively. In (**B**), green fluorescence indicates EdU-positive nuclei and blue fluorescence indicates Hoechst-stained nuclei. Dashed lines in (**D**) mark the wound boundaries. In (**C**), bar colors identify the KI concentrations shown on the x-axis; in (**E**), blue and purple bars denote the control and KI groups, respectively. *** $p < 0.001$; **** $p < 0.0001$.

3.2. Changes in PI3K/AKT/mTOR Pathway-Related Proteins After KI Exposure

Compared with the control, the 10^{-5}, 10^{-3}, and 10^{-1} mmol/L KI groups showed increased PI3K, p-PI3K, mTOR, and p-P70S6K signals and decreased PTEN signal. p-AKT, p-mTOR, and P70S6K signals increased in the 10^{-3} and 10^{-1} mmol/L groups, while total AKT increased in the 10^{-5} and 10^{-3} mmol/L groups (all $p < 0.05$; Figure 2). Thus, KI exposure was accompanied by reduced PTEN and increased loading control-normalized signals for several PI3K/AKT/mTOR-related proteins. At 10^{-3} mmol/L KI, the p-AKT/AKT and p-P70S6K/P70S6K ratios were higher than in the control (adjusted $p < 0.0001$ and $p = 0.0003$, respectively). The p-P70S6K/P70S6K ratio was also higher at 10^{-1} mmol/L (adjusted $p = 0.0179$). The p-mTOR/mTOR ratio did not differ significantly from the control at any tested concentration (all adjusted $p > 0.05$; Figure 2K).

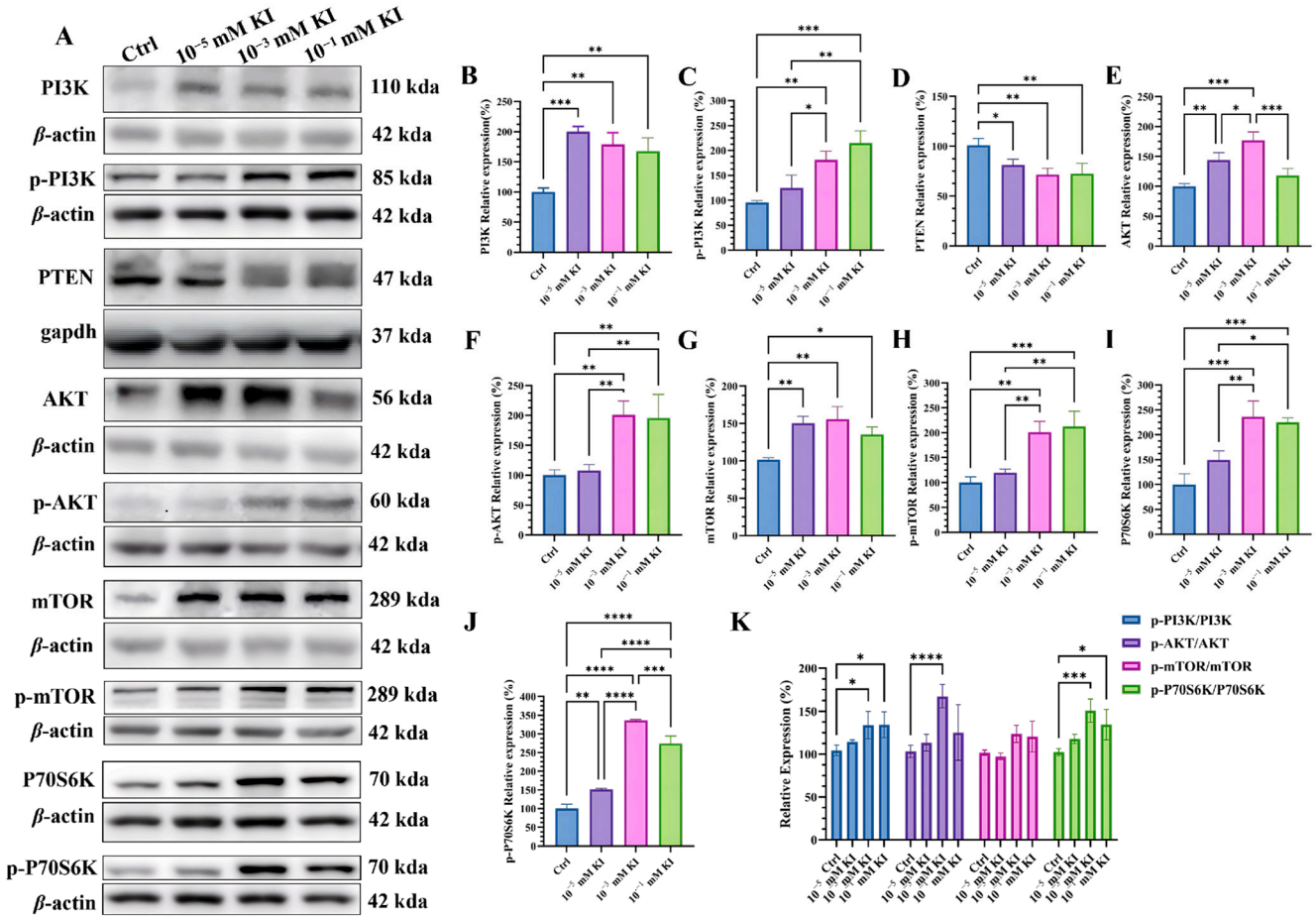


Figure 2. PTEN and PI3K/AKT/mTOR-related protein signals after exposure to different KI concentrations. (**A**) Representative Western blots after 48 h of treatment with vehicle or 10^{-5}, 10^{-3}, or 10^{-1} mmol/L KI. (**B**–**J**) Relative signals for PI3K, p-PI3K, PTEN, AKT, p-AKT, mTOR, p-mTOR, P70S6K, and p-P70S6K, respectively. GAPDH was the loading control for PTEN, and β-actin was used for the other targets; signals were normalized to the control. The PI3K label denotes the p110α catalytic-subunit signal detected with CST #4249; p-PI3K denotes an approximately 85 kDa signal detected using the phospho-p85/p55 antibody CST #4228, which recognizes p85 Tyr458/p55 Tyr199. Phosphorylated and total proteins were each normalized to the loading control. Data are mean ± SD from three independent experiments ($n = 3$). Panels (**B**–**J**) were analyzed by a one-way ANOVA with Tukey's multiple-comparisons test. Brackets indicate comparisons. * $p < 0.05$; ** $p < 0.01$; *** $p < 0.001$; **** $p < 0.0001$. (**K**) The cross-subunit p85-reactive/p110α signal ratio and matched ratios of p-AKT/AKT, p-mTOR/mTOR, and p-P70S6K/P70S6K calculated from paired measurements within independent experiments. The ratio analysis used ordinary two-way ANOVA with treatment and protein ratio as factors, followed by Dunnett's comparisons against the control within each

ratio; adjusted p values are reported. The p-PI3K/PI3K label in the plot denotes a cross-subunit p85-reactive/p110α signal ratio; it is not a matched phospho-to-total ratio and was not used to infer PI3K phosphorylation stoichiometry.

3.3. Cell Cycle Changes After KI Exposure

Flow cytometry showed that the proportions of S-phase cells and SPF were higher in the 10^{-5}, 10^{-3}, and 10^{-1} mmol/L KI groups than in the control, with the highest means in the 10^{-3} mmol/L group. PI was increased in the 10^{-5} and 10^{-3} mmol/L groups (all $p < 0.05$; Figure 3A–C). Cyclin D1 expression was higher in all KI groups than in the control, with the highest mean in the 10^{-3} mmol/L group (all $p < 0.05$; Figure 3D,E). These findings show that increased DNA synthesis occurred alongside changes in cell cycle distribution and increased Cyclin D1 expression.

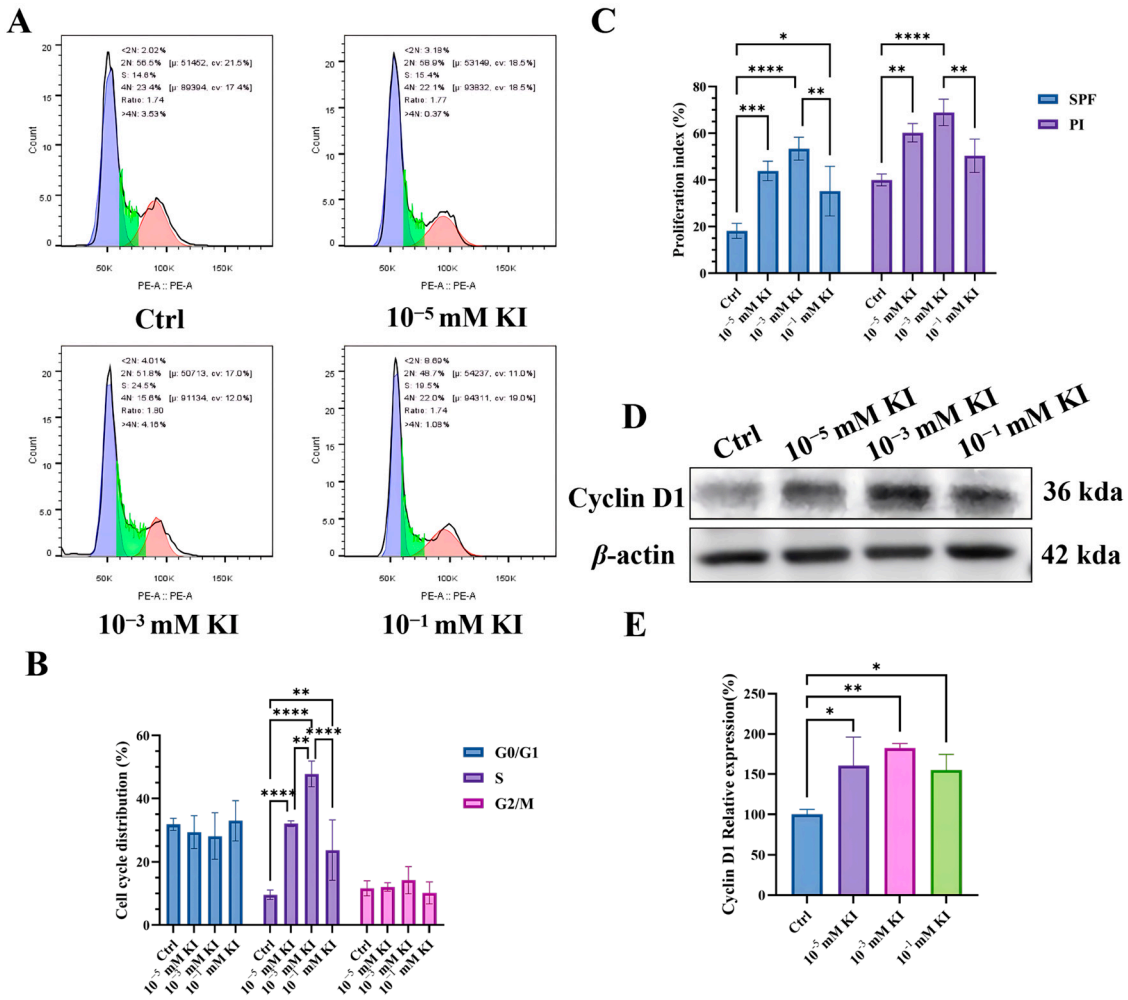


Figure 3. Cell cycle indices and Cyclin D1 expression after exposure to different KI concentrations. (**A**) Representative flow cytometry plots after 48 h of treatment with vehicle or 10^{-5}, 10^{-3}, or 10^{-1} mmol/L KI. (**B**) Distribution of cells in G_0/G_1, S, and G_2/M phases. (**C**) S-phase fraction (SPF) and proliferation index (PI); calculation formulas are provided in Section 2.6. (**D**) Representative Cyclin D1 Western blot, with β-actin as the loading control. (**E**) Relative Cyclin D1 expression normalized to the loading control and control group. Data are mean ± SD from three independent experiments ($n = 3$). Panel (**B**) was analyzed by an ordinary two-way ANOVA with KI concentration and cell cycle phase as factors, followed by Tukey's comparisons within each phase. Panel (**C**) was analyzed by an ordinary two-way ANOVA with KI concentration and index type as factors, followed by Šídák's comparisons within each index. Panel (**E**) was analyzed by a one-way ANOVA with

Tukey's multiple-comparisons test. Brackets indicate comparisons. * $p < 0.05$; ** $p < 0.01$; *** $p < 0.001$; **** $p < 0.0001$. In (**A**), purple, green, and pink/red shading indicates the G0/G1, S, and G2/M components, respectively. In (**B**), blue, purple, and pink bars indicate G0/G1, S, and G2/M, respectively; in (**C**), blue and purple bars indicate SPF and PI, respectively.

3.4. Combined LY294002 Treatment Reduces DNA Synthesis and Wound Closure Under KI Exposure

The CCK-8 results from the LY294002 single-agent concentration screen are shown in Figure 4A. Subsequent intervention experiments used 10 μmol/L LY294002 together with 10^{-3} mmol/L KI. EdU positivity was higher in the KI group than in the control; it was lower in the LY+KI group than in the KI group and also lower than in the control (Figure 4B,C). In the wound-healing assay, the 48 h closure rate increased in the KI group, whereas it was lower in the LY+KI group than in both the KI and control groups (Figure 4D,E). Statistical significance for each comparison is indicated by brackets in the figure.

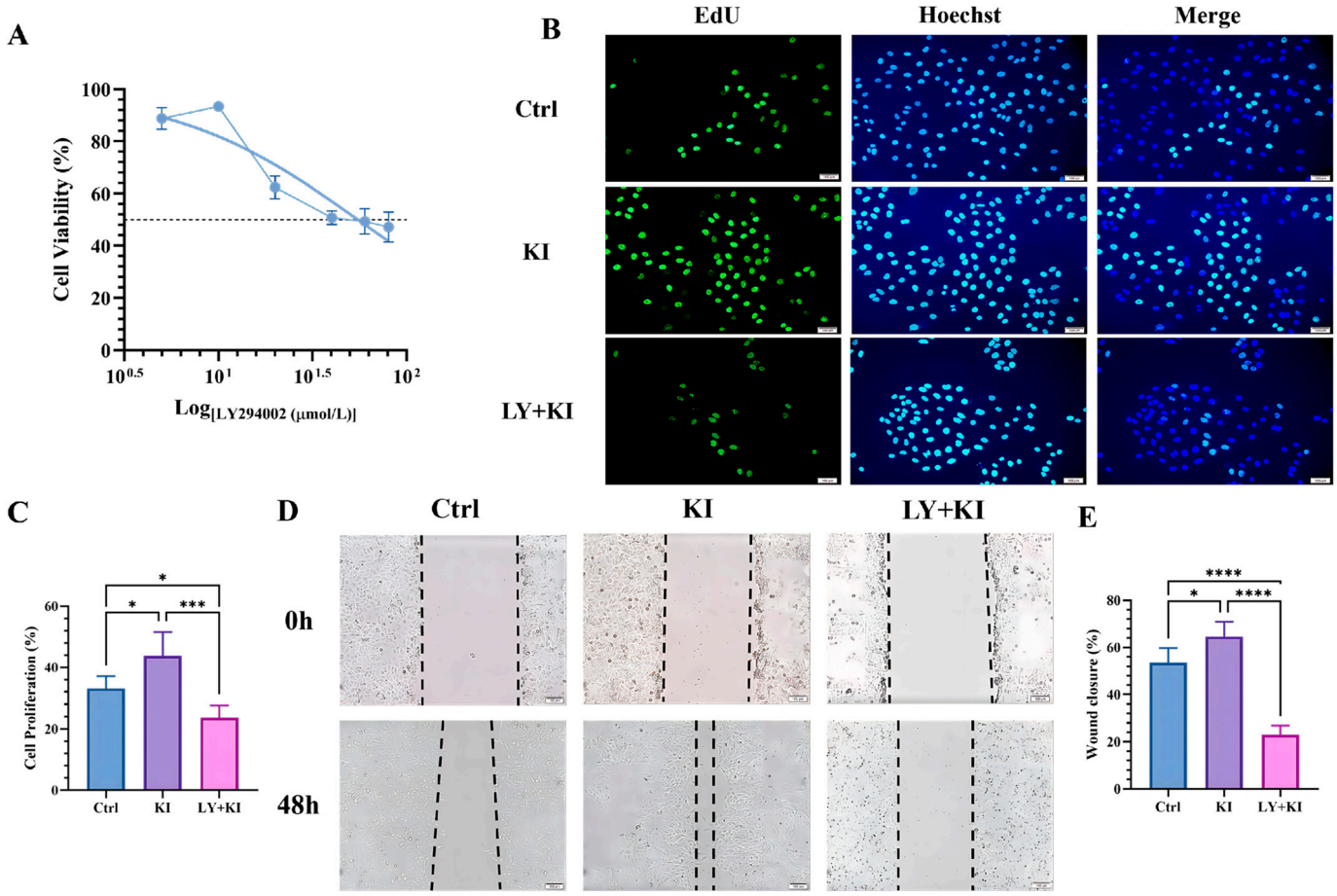


Figure 4. Effects of combined LY294002 treatment on DNA synthesis and wound closure under KI exposure. (**A**) CCK-8 screen after 48 h of single-agent LY294002 exposure; the *x*-axis is logarithmic, and data are mean ± SD. (**B**,**C**) Representative EdU images and percentage of EdU-positive cells in Ctrl, KI, and LY+KI groups. (**D**,**E**) Representative wound images at 0 and 48 h and the wound-closure rate at 48 h in the three groups. Scale bars in (**B**,**D**), 100 μm. Data in (**C**,**E**) are shown as bar plots representing mean ± SD. The KI group received 10^{-3} mmol/L KI for 48 h; the LY+KI group received 10 μmol/L LY294002 and 10^{-3} mmol/L KI simultaneously for 48 h. Each experiment was independently repeated three times ($n = 3$). Panels (**A**,**C**,**E**) were analyzed by a one-way ANOVA with Tukey's multiple-comparisons test. Brackets indicate comparisons. * $p < 0.05$; *** $p < 0.001$; **** $p < 0.0001$. Green fluorescence in (**B**) indicates EdU-positive nuclei, and blue fluorescence indicates Hoechst-stained

nuclei. The horizontal dashed line in (**A**) indicates 50% relative viability; dashed lines in (**D**) mark the wound boundaries. In (**C**,**E**), blue, purple, and pink bars denote Ctrl, KI, and LY+KI, respectively.

3.5. Combined LY294002 Treatment Alters KI-Associated Pathway Protein Responses

Compared with the control, the KI group showed increased signals for PI3K, p-PI3K, AKT, p-AKT, mTOR, p-mTOR, P70S6K, and p-P70S6K and decreased PTEN signal. Compared with the KI group, the LY+KI group showed lower signals for these pathway-related proteins and higher PTEN signal (all $p < 0.05$; Figure 5). These coordinated protein changes accompanied the lower DNA synthesis and wound closure observed with combined LY294002 treatment. Compared with KI alone, LY+KI reduced p-AKT/AKT, p-mTOR/mTOR, and p-P70S6K/P70S6K (adjusted $p = 0.0006$, $p = 0.0366$, and $p < 0.0001$, respectively; Figure 5K). Relative to the control, KI increased p-AKT/AKT and p-P70S6K/P70S6K (adjusted $p = 0.0073$ and $p = 0.0008$), whereas p-mTOR/mTOR was not significantly different (adjusted $p = 0.6519$).

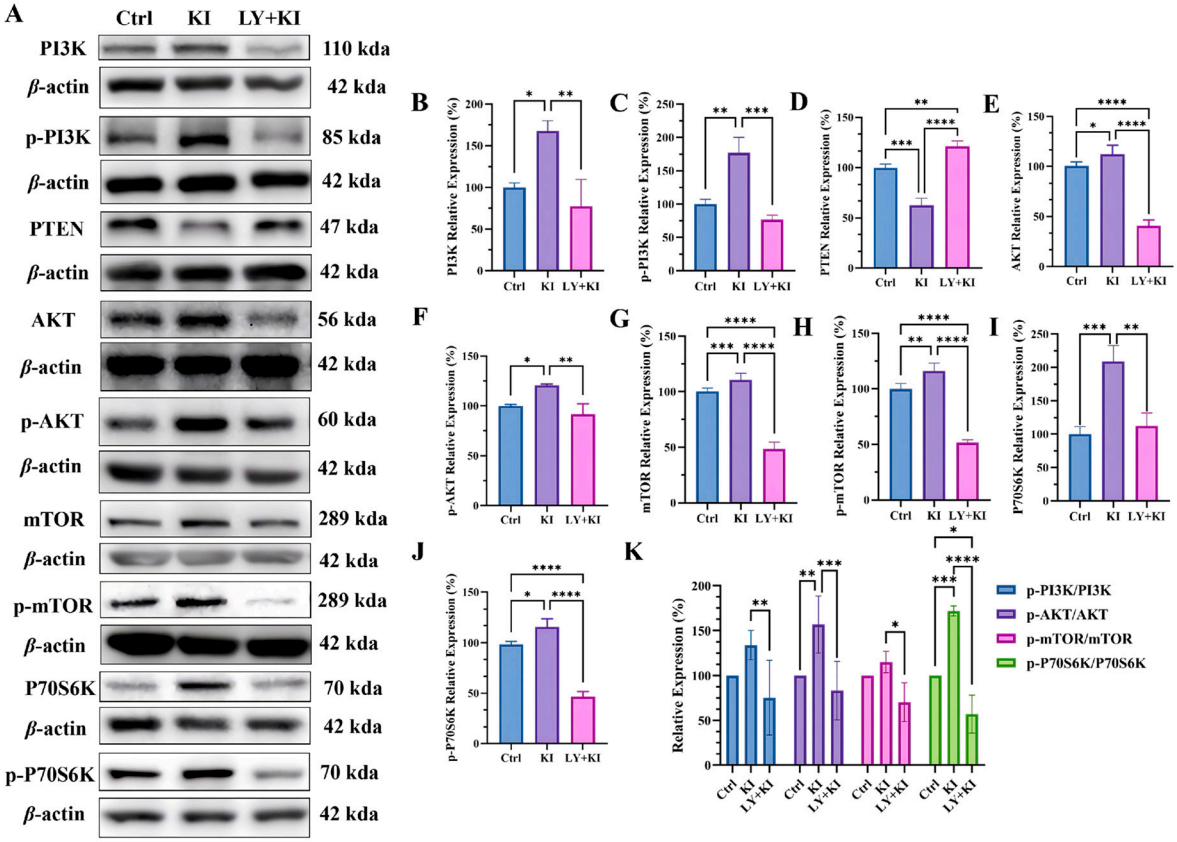


Figure 5. PI3K/AKT/mTOR-related protein responses after combined LY294002 treatment. (**A**) Representative Western blots for Ctrl, KI, and LY+KI groups. (**B**–**J**) Relative signals for PI3K, p-PI3K, PTEN, AKT, p-AKT, mTOR, p-mTOR, P70S6K, and p-P70S6K, respectively. The KI group received 10^{-3} mmol/L KI for 48 h; the LY+KI group received 10 μmol/L LY294002 and 10^{-3} mmol/L KI simultaneously for 48 h. *β*-actin was the loading control, and signals were normalized to the loading control and control group. PI3K denotes p110α detected with CST #4249, whereas p-PI3K denotes an approximately 85 kDa signal detected using the phospho-p85/p55 antibody CST #4228 (p85 Tyr458/p55 Tyr199); phosphorylated and total proteins were each normalized to the loading control. Data are mean ± SD from three independent experiments ($n = 3$). Panels (**B**–**J**) were analyzed by a one-way ANOVA with Tukey's multiple-comparisons test. Brackets indicate comparisons. * $p < 0.05$; ** $p < 0.01$; *** $p < 0.001$; **** $p < 0.0001$. (**K**) The cross-subunit p85-reactive/p110α signal ratio and matched ratios of p-AKT/AKT, p-mTOR/mTOR, and p-P70S6K/P70S6K calculated from paired measurements within independent experiments. The ratio analysis used ordinary two-way ANOVA

with treatment and protein ratio as factors, followed by Tukey's multiple comparisons within each ratio; adjusted p values are reported. The p-PI3K/PI3K label in the plot denotes a cross-subunit p85-reactive/p110α signal ratio; it is not a matched phospho-to-total ratio and was not used to infer PI3K phosphorylation stoichiometry.

3.6. Combined LY294002 Treatment Affects Cell Cycle Distribution

Compared with the control, the KI group showed increased SPF and PI, a lower proportion of G_0/G_1-phase cells, and a higher proportion of S-phase cells. Compared with the KI group, the LY+KI group showed lower SPF and PI, a higher G_0/G_1 fraction, and a lower S-phase fraction (all $p < 0.05$; Figure 6A–C). Cyclin D1 was increased in the KI group relative to the control, but was lower in the LY+KI group than in both the KI and control groups (all $p < 0.05$; Figure 6D,E). Thus, reduced DNA synthesis after combined LY294002 treatment occurred alongside changes in cell cycle distribution and Cyclin D1 expression.

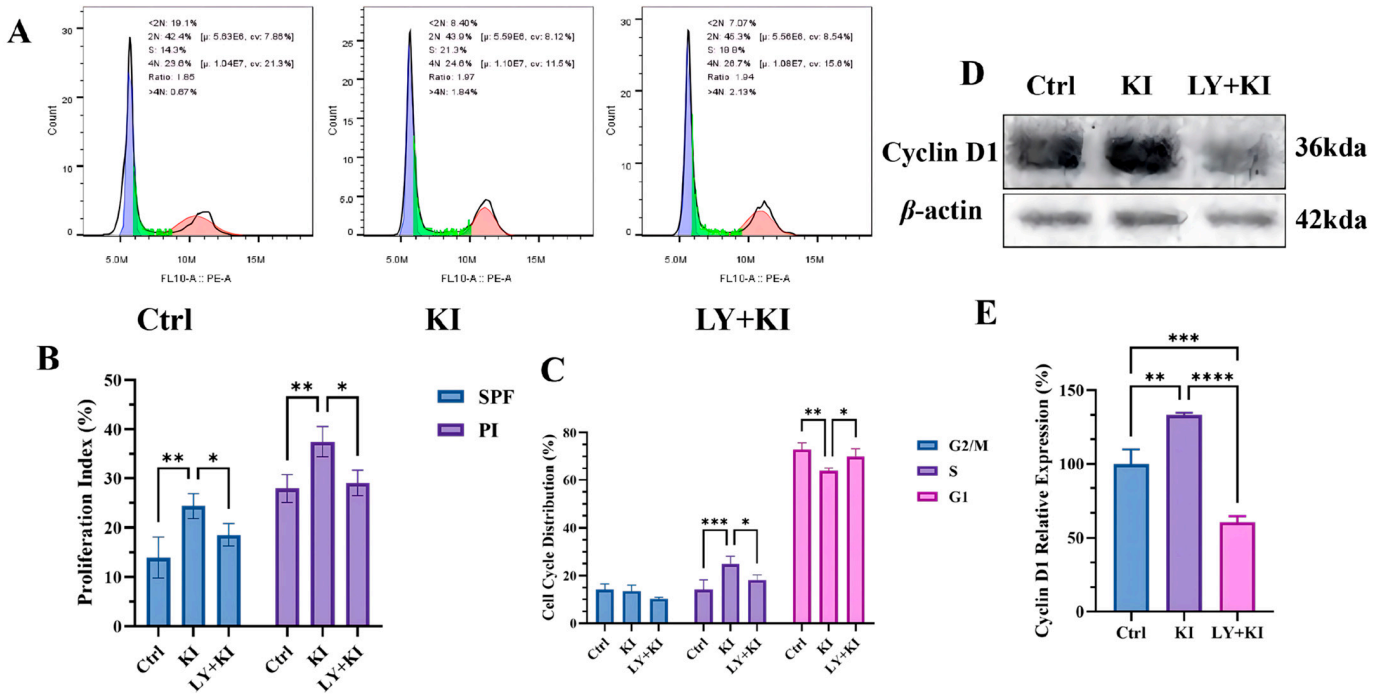


Figure 6. Cell cycle distribution and Cyclin D1 expression after combined LY294002 treatment. (**A**) Representative flow-cytometry plots for Ctrl, KI, and LY+KI groups. (**B**) S-phase fraction (SPF) and proliferation index (PI); calculation formulas are provided in Section 2.6. (**C**) Cell cycle distribution; phases are shown in the order G_2/M, S, and G_0/G_1, as indicated in the figure. (**D**) Representative Cyclin D1 Western blot, with β-actin as the loading control. (**E**) Relative Cyclin D1 expression normalized to the loading control and control group. The KI group received 10^{-3} mmol/L KI for 48 h; the LY+KI group received 10 μmol/L LY294002 and 10^{-3} mmol/L KI simultaneously for 48 h. Data are mean ± SD from three independent experiments ($n = 3$). Panel (**B**) was analyzed by two-way repeated-measures ANOVA, matching treatment and index type within independent experiments, followed by Šídák's comparisons within each index. Panel (**C**) was analyzed by an ordinary two-way ANOVA followed by Tukey's comparisons within each phase. Panel (**E**) was analyzed by a one-way ANOVA with Tukey's multiple-comparisons test. Brackets indicate comparisons. * $p < 0.05$; ** $p < 0.01$; *** $p < 0.001$; **** $p < 0.0001$. In (**A**), purple, green, and pink/red shading indicates the G0/G1, S, and G2/M components, respectively. In (**B**), blue and purple bars indicate SPF and PI, respectively. In (**C**), blue, pink, and purple bars indicate G2/M, S, and G0/G1, respectively; in (**E**), these colors denote Ctrl, KI, and LY+KI, respectivel.

4. Discussion

The increasing burden of thyroid cancer has sustained interest in the relationship between environmental exposures and tumor biology. Iodine is essential for thyroid hormone synthesis and is also an environmental factor to which thyroid cells are directly exposed. In some regions with high-iodine water, drinking water can be a sustained source of exposure [13,18]. Retrospective studies in high-water-iodine areas of China have examined the relationship between water iodine exposure and thyroid cancer at the population level [31], while recent meta-analyses have also suggested an association between urinary iodine and thyroid cancer risk [12]. Against this background, investigating iodine effects on the proliferation and related signaling of established tumor cells may help clarify links between environmental exposure and tumor progression. In RET/PTC1-rearranged TPC-1 cells, we observed that a specific KI concentration increased DNA synthesis and wound closure, accompanied by changes in PI3K/AKT/mTOR-related signals, Cyclin D1, and cell cycle distribution. These linked phenotypic and molecular observations provide a basis for further mechanistic analysis in this defined cell model.

The effects of KI in this study varied with concentration and exposure time. At 48 h, the 10^{-3} mmol/L group had the highest mean cell viability, whereas the 10 mmol/L group showed a decrease, indicating a non-monotonic concentration-response pattern under the conditions tested. EdU results further supported the proliferative response to 10^{-5} and 10^{-3} mmol/L KI. In previous work, Lv et al. treated BRAF V600E-mutant papillary thyroid carcinoma BCPAP cells and anaplastic thyroid carcinoma 8305C cells with 2 μmol/L KIO_3 for 72 h and observed increased DNA synthesis and cell cycle changes [21]. Fuziwara et al. reported that high iodine suppressed Notch/miR-19-related responses and restored TGF-β-mediated inhibitory signaling in a BRAF-driven thyroid follicular cell model [10]. Together, these findings suggest that the iodine compound, concentration, exposure duration, and molecular background of the cells can influence the direction of the response. By using KI over a broad concentration range, the present study identified conditions under which proliferative responses were observed in TPC-1 cells, providing a defined phenotypic basis for subsequent pathway analyses.

PI3K/AKT signaling is shaped by both growth-promoting inputs and negative regulation. PI3K promotes the conversion of phosphatidylinositol 4,5-bisphosphate to phosphatidylinositol 3,4,5-trisphosphate (PIP_3), whereas PTEN constrains this process by dephosphorylating PIP_3; PTEN lipid-phosphatase activity is a central basis for its regulation of cell growth [32]. In this study, KI exposure was associated with reduced PTEN expression and increased PI3K and p-PI3K signals, together with increased p-AKT. The coordinated changes in positive and negative regulators provide a plausible context for the increase in AKT-related signaling after KI exposure and identify PTEN as an iodine-responsive molecule of interest. The opposite-direction changes in PTEN and pathway-related protein signals after combined LY294002 treatment are consistent with this signaling association.

Downstream of AKT, mTOR links growth stimulation to cellular anabolism. Mechanistic studies have shown that AKT-mediated phosphorylation regulates TSC2, weakening the inhibitory effect of the TSC complex on Rheb and thereby promoting mTOR-related signaling. Rheb lies downstream of TSC1/TSC2 and upstream of mTOR and participates in the regulation of S6K and 4E-BP1 [33,34]. P70S6K, a downstream effector of mTORC1, is an important link between growth signals and protein synthesis [19]. In the present study, KI increased both loading-control-normalized phosphoprotein signals and the p-AKT/AKT and p-P70S6K/P70S6K ratios at 10^{-3} mmol/L. In contrast, p-mTOR/mTOR did not increase significantly, indicating that the higher p-mTOR signal partly accompanied changes in total mTOR abundance. Combined LY294002 treatment reduced all three ratios relative to KI alone. These results support an AKT/P70S6K-associated phosphorylation

response without establishing uniform activation at every measured pathway node. These findings place changes in the CCK-8 signal and DNA synthesis alongside changes in proteins within a growth-regulatory network. Together, these results support the involvement of PI3K/AKT/mTOR-related signaling in the proliferative response of TPC-1 cells to KI. Previous work has also used LY294002 in TPC-1 cells to investigate PI3K/AKT-associated signaling in PTC [35].

Cyclin D1 is an important regulator linking extracellular growth stimuli to the G_1/S transition. Its complex with CDK4/6 participates in retinoblastoma protein (RB)-related regulation and cell cycle progression [36]. AKT can also affect Cyclin D1 beyond transcription: GSK-3β promotes Cyclin D1 degradation, and PI3K/AKT-related signaling can influence Cyclin D1 stability through inhibition of GSK-3β [37]. In our study, increased Cyclin D1 coincided with higher EdU positivity, SPF, and PI; these measures decreased after combined LY294002 treatment, alongside an increase in the G_0/G_1 fraction. The concordant changes support the participation of Cyclin D1-related cell cycle regulation in the proliferative response to KI. Compared with previous work on high-iodine regulation of AKT/Wee1/CDK1 [21], the present study adds evidence related to mTOR/P70S6K and Cyclin D1, suggesting that iodine exposure may alter thyroid cancer cell proliferation through multiple cell cycle regulatory nodes.

PI3K/AKT-related signaling has been implicated in PTC motility and invasive phenotypes. Yu et al. reported that IRS1 can promote thyroid cancer metastasis through PI3K/AKT and epithelial–mesenchymal transition-related processes [20], and a 2026 study linked the RAN–S100A10–EGFR axis to PI3K/AKT signaling and PTC cell invasiveness [38]. In the present study, KI increased 48 h wound closure, whereas combined LY294002 treatment reduced it. The parallel changes in wound closure and proliferative measures suggest that KI affects cellular behaviors relevant to tumor expansion.

Iodine may also regulate PTC cells through processes that operate in parallel with PI3K/AKT/mTOR. Huang et al. found that SLC34A2 upregulation and SLC4A4 downregulation in PTC tissue were associated with higher urinary iodine and linked these transporters to MAPK signaling, invasion, and migration through functional experiments [39]. In 2024, Li et al. reported regulation of malignant phenotypes in PTC under high-iodine conditions through the circ_0004851/miR-296-3p/FGF11 axis [40]. BRAF-associated autophagy has also been implicated in cellular responses to iodine exposure [22]. Together, these studies indicate that iodine-related effects may converge on multiple networks regulating cell growth, involving transporters, noncoding RNAs, and cellular stress responses. By focusing on PTEN, PI3K/AKT/mTOR/P70S6K, and Cyclin D1, the present study adds observations from a RET/PTC1-rearranged model to this broader picture of pathway regulation.

The RET/PTC1 background defines the molecular scope of this study. PTC contains distinct driver-defined subgroups with different signaling features [23], and recent reviews describe the diversity of RET fusions and their associated signaling and therapeutic responses [41,42]. In TPC-1 and CUTC48 CCDC6–RET models, enhanced AKT–mTOR signaling has been associated with selpercatinib resistance, with mTOR inhibition reducing cell growth [24]. These findings highlight AKT–mTOR signaling as a biologically relevant network in RET-fusion models. Our study extends this context by examining the response to KI and linking protein changes with DNA synthesis and cell cycle regulation in TPC-1 cells.

The present study provides a basis for further mechanistic and exposure-oriented investigation. Most endpoints were measured at 48 h in a single RET/PTC1-rearranged cell line; denser time courses and additional RET-fusion and other PTC models would help define the sequence and molecular context of the responses. The combined-treatment design did not include a matched LY294002-only group. Adding this group, together with genetic perturbation or a second, more selective inhibitor, would distinguish basal drug effects

from KI-dependent responses and strengthen pathway attribution. Proliferation-controlled migration assays would further clarify the contribution of cell movement to wound closure. For exposure translation, 10^{-3} mmol/L KI corresponds to 1 μmol/L iodide, or approximately 127 μg iodine/L in the added solution. This nominal medium concentration is distinct from drinking water concentration and thyroid tissue dose. Iodide kinetic models account for absorption, distribution, renal elimination, and thyroid uptake [43]; combining such models with measured extracellular and intracellular iodine and functional uptake in TPC-1 cells would provide a quantitative basis for comparing the experimental exposure with human iodine intake. In vivo validation would then help assess the relevance of these cellular findings to thyroid tumor progression.

5. Conclusions

KI exerted concentration- and time-dependent effects on RET/PTC1-rearranged TPC-1 cells. At 10^{-3} mmol/L for 48 h, KI increased DNA synthesis and wound closure, accompanied by reduced PTEN, increased p-AKT/AKT and p-P70S6K/P70S6K ratios, increased Cyclin D1, and changes in cell cycle distribution. Combined LY294002 treatment attenuated these cellular responses and shifted the cell cycle distribution toward G_0/G_1. These findings support the involvement of PI3K/AKT/mTOR-related signaling and Cyclin D1-associated cell cycle regulation in the proliferative response of TPC-1 cells to KI.

Author Contributions: Conceptualization, Y.C. and H.L.; methodology, Y.C.; software, S.L.; validation, S.L.; formal analysis, S.L., X.Y., P.D. and Z.X.; investigation, S.L., P.D. and Z.X.; resources, H.L.; data curation, S.L., X.Y., P.D. and Z.X.; writing—original draft preparation, S.L. and P.D.; writing—review and editing, Y.C.; visualization, S.L. and P.D.; supervision, Y.C.; project administration, H.L.; funding acquisition, X.Y., Y.C. and H.L. All authors have read and agreed to the published version of the manuscript.

Funding: This research was funded by the National Natural Science Foundation of China (82173641); the Key Laboratory of Environment and Health, Ministry of Education, Huazhong University of Science and Technology (2021GWKFJJ03); the Tianjin High-Level Talent Training Program (TJSQNYXXR-D2-151); and the Tianjin Health Science and Technology Project (TJWJ2023QN095).

Institutional Review Board Statement: Not applicable. This study used a commercially obtained established human thyroid cancer cell line (TPC-1) and did not involve recruitment of human participants, collection of primary human specimens, or animal experiments.

Informed Consent Statement: Not applicable. This study did not involve human participants or identifiable patient information.

Data Availability Statement: The data supporting the findings of this study are available from the corresponding authors upon reasonable request.

Acknowledgments: During manuscript preparation and revision, the authors used ChatGPT-6 and Codex 2026 (OpenAI) to assist with language editing, presentation of author-provided results, preparation of responses to reviewers, and development of the graphical abstract. The authors reviewed and edited the resulting content and take full responsibility for the final manuscript.

Conflicts of Interest: The authors declare no conflicts of interest.

References

1. Sung, H.; Ferlay, J.; Siegel, R.L.; Laversanne, M.; Soerjomataram, I.; Jemal, A.; Bray, F. Global Cancer Statistics 2020: GLOBOCAN Estimates of Incidence and Mortality Worldwide for 36 Cancers in 185 Countries. *CA Cancer J. Clin.* **2021**, *71*, 209–249. [CrossRef] [PubMed]
2. Han, B.; Zheng, R.; Zeng, H.; Wang, S.; Sun, K.; Chen, R.; Li, L.; Wei, W.; He, J. Cancer incidence and mortality in China, 2022. *J. Natl. Cancer Cent.* **2024**, *4*, 47–53. [CrossRef] [PubMed]

3. Araque, D.V.P.; Bleyer, A.; Brito, J.P. Thyroid cancer in adolescents and young adults. *Future Oncol.* **2017**, *13*, 1253–1261. [CrossRef] [PubMed]
4. Aschebrook-Kilfoy, B.; Ward, M.H.; Sabra, M.M.; Devesa, S.S. Thyroid Cancer Incidence Patterns in the United States by Histologic Type, 1992–2006. *Thyroid* **2011**, *21*, 125–134. [CrossRef] [PubMed]
5. Chen, D.W.; Lang, B.H.H.; McLeod, D.S.A.; Newbold, K.; Haymart, M.R. Thyroid cancer. *Lancet* **2023**, *401*, 1531–1544. [CrossRef] [PubMed]
6. Kitahara, C.M.; Sosa, J.A. The changing incidence of thyroid cancer. *Nat. Rev. Endocrinol.* **2016**, *12*, 646–653. [CrossRef] [PubMed]
7. Bath, S.C. Thyroid function and iodine intake: Global recommendations and relevant dietary trends. *Nat. Rev. Endocrinol.* **2024**, *20*, 474–486. [CrossRef] [PubMed]
8. Sohn, S.Y.; Inoue, K.; Rhee, C.M.; Leung, A.M. Risks of Iodine Excess. *Endocr. Rev.* **2024**, *45*, 858–879. [CrossRef] [PubMed]
9. Wang, H.; Jiang, Y.; Song, J.; Liang, H.; Liu, Y.; Huang, J.; Yin, P.; Wu, D.; Zhang, H.; Liu, X.; et al. The risk of perchlorate and iodine on the incidence of thyroid tumors and nodular goiter: A case-control study in southeastern China. *Environ. Health* **2022**, *21*, 4. [CrossRef] [PubMed]
10. Fuziwara, C.S.; Kimura, E.T. High Iodine Blocks a Notch/miR-19 Loop Activated by the BRAF V600E Oncoprotein and Restores the Response to TGFβ in Thyroid Follicular Cells. *Thyroid* **2014**, *24*, 453–462. [CrossRef] [PubMed]
11. Lee, J.H.; Hwang, Y.; Song, R.Y.; Yi, J.W.; Yu, H.W.; Kim, S.; Chai, Y.J.; Choi, J.Y.; Lee, K.E.; Park, S.K. Relationship between iodine levels and papillary thyroid carcinoma: A systematic review and meta-analysis. *Head Neck* **2017**, *39*, 1711–1718. [CrossRef] [PubMed]
12. Li, S.; Yu, H. Dietary and Urinary Iodine in Relation to Thyroid Cancer Risk: A Meta-Analysis. *Cancer Control* **2026**, *33*, 10732748261419192. [CrossRef] [PubMed]
13. Ma, R.; Yan, M.; Han, P.; Wang, T.; Li, B.; Zhou, S.; Zheng, T.; Hu, Y.; Borthwick, A.G.L.; Zheng, C.; et al. Deficiency and excess of groundwater iodine and their health associations. *Nat. Commun.* **2022**, *13*, 7354. [CrossRef] [PubMed]
14. Kassim, I.A.R.; Moloney, G.; Busili, A.; Nur, A.Y.; Paron, P.; Jooste, P.; Gadain, H.; Seal, A.J. Iodine Intake in Somalia Is Excessive and Associated with the Source of Household Drinking Water. *J. Nutr.* **2014**, *144*, 375–381. [CrossRef] [PubMed]
15. Cui, Y.; Wang, Y.; Zhang, D.; Duan, Y.; Li, W.; Li, F.; Chen, L. How did we eliminate the hazards of water-borne excessive iodine in northern China? *Ecotoxicol. Environ. Saf.* **2024**, *269*, 115795. [CrossRef] [PubMed]
16. Watts, M.J.; Middleton, D.R.S.; Marriott, A.; Humphrey, O.S.; Hamilton, E.; McCormack, V.; Menya, D.; Farebrother, J.; Osano, O. Iodine status in western Kenya: A community-based cross-sectional survey of urinary and drinking water iodine concentrations. *Environ. Geochem. Health* **2019**, *42*, 1141–1151. [CrossRef] [PubMed]
17. Hou, X.; Zhao, M.; Li, J.; Du, Y.; Li, M.; Liu, L.; Liu, P.; Meng, F.; Fan, L.; Shen, H.; et al. Distribution of iodine concentration in drinking water in China mainland and influence factors of its variation. *Sci. Total Environ.* **2023**, *892*, 164628. [CrossRef] [PubMed]
18. Shen, H.; Liu, S.; Sun, D.; Zhang, S.; Su, X.; Shen, Y.; Han, H. Geographical distribution of drinking-water with high iodine level and association between high iodine level in drinking-water and goitre: A Chinese national investigation. *Br. J. Nutr.* **2011**, *106*, 243–247. [CrossRef] [PubMed]
19. Glaviano, A.; Foo, A.S.C.; Lam, H.Y.; Yap, K.C.H.; Jacot, W.; Jones, R.H.; Eng, H.; Nair, M.G.; Makvandi, P.; Geoerger, B.; et al. PI3K/AKT/mTOR signaling transduction pathway and targeted therapies in cancer. *Mol. Cancer* **2023**, *22*, 138. [CrossRef] [PubMed]
20. Yu, F.; Huang, D.; Kuang, Y.; Dong, J.; Han, Q.; Zhou, J.; Teng, X. IRS1 promotes thyroid cancer metastasis through EMT and PI3K/AKT pathways. *Clin. Endocrinol.* **2024**, *100*, 284–293. [CrossRef] [PubMed]
21. Lv, C.; Gao, Y.; Yao, J.; Li, Y.; Lou, Q.; Zhang, M.; Tian, Q.; Yang, Y.; Sun, D. High Iodine Induces the Proliferation of Papillary and Anaplastic Thyroid Cancer Cells via AKT/Wee1/CDK1 Axis. *Front. Oncol.* **2021**, *11*, 622085. [CrossRef] [PubMed]
22. Zhang, D.; Xu, X.; Li, J.; Yang, X.; Sun, J.; Wu, Y.; Qiao, H. High iodine effects on the proliferation, apoptosis, and migration of papillary thyroid carcinoma cells as a result of autophagy induced by BRAF kinase. *Biomed. Pharmacother.* **2019**, *120*, 109476. [CrossRef] [PubMed]
23. Cancer Genome Atlas Research Network. Integrated Genomic Characterization of Papillary Thyroid Carcinoma. *Cell* **2014**, *159*, 676–690. [CrossRef] [PubMed]
24. Amitani, M.; Shimizu, T.; Oba, T.; Kawamura, M.; Ito, K.-I. Activation of the AKT-mTOR pathway confers selpercatinib resistance in thyroid cancer cells harboring the CCDC6-RET fusion gene. *Biochem. Biophys. Rep.* **2025**, *43*, 102136. [CrossRef] [PubMed]
25. Ratajczak, M.; Gaweł, D.; Godlewska, M. Novel Inhibitor-Based Therapies for Thyroid Cancer—An Update. *Int. J. Mol. Sci.* **2021**, *22*, 11829. [CrossRef] [PubMed]
26. Landa, I.; Pozdeyev, N.; Korch, C.; Marlow, L.A.; Smallridge, R.C.; Copland, J.A.; Henderson, Y.C.; Lai, S.Y.; Clayman, G.L.; Onoda, N.; et al. Comprehensive Genetic Characterization of Human Thyroid Cancer Cell Lines: A Validated Panel for Preclinical Studies. *Clin. Cancer Res.* **2019**, *25*, 3141–3151. [CrossRef] [PubMed]

27. Mielecki, D.; Gajda, E.; Sikorska, J.; Betkowska, A.; Rozwadowski, M.; Gawel, A.M.; Kulecka, M.; Zeber-Lubecka, N.; Godlewska, M.; Gawel, D. Resolving the role of podoplanin in the motility of papillary thyroid carcinoma-derived cells using RNA sequencing. *Comput. Struct. Biotechnol. J.* **2023**, *21*, 3810–3826. [CrossRef] [PubMed]
28. Vlahos, C.J.; Matter, W.F.; Hui, K.Y.; Brown, R. A specific inhibitor of phosphatidylinositol 3-kinase, 2-(4-morpholinyl)-8-phenyl-4H-1-benzopyran-4-one (LY294002). *J. Biol. Chem.* **1994**, *269*, 5241–5248. [CrossRef]
29. Walker, E.H.; Pacold, M.E.; Perisic, O.; Stephens, L.; Hawkins, P.T.; Wymann, M.P.; Williams, R.L. Structural Determinants of Phosphoinositide 3-Kinase Inhibition by Wortmannin, LY294002, Quercetin, Myricetin, and Staurosporine. *Mol. Cell* **2000**, *6*, 909–919. [CrossRef] [PubMed]
30. Davies, S.P.; Reddy, H.; Caivano, M.; Cohen, P. Specificity and mechanism of action of some commonly used protein kinase inhibitors. *Biochem. J.* **2000**, *351*, 95–105. [CrossRef]
31. Chen, Y.; Lv, C.; Zhang, X.; Yang, K.; Li, J.; Shen, Z.; Ai, L.; Sun, D.; Zhang, W. Association between different water iodine exposures and thyroid cancer: A retrospective study of high water iodine areas in China from 2009 to 2020. *Chemosphere* **2024**, *346*, 140581. [CrossRef] [PubMed]
32. Maehama, T.; Dixon, J.E. The Tumor Suppressor, PTEN/MMAC1, Dephosphorylates the Lipid Second Messenger, Phosphatidylinositol 3,4,5-Trisphosphate. *J. Biol. Chem.* **1998**, *273*, 13375–13378. [CrossRef] [PubMed]
33. Inoki, K.; Li, Y.; Zhu, T.; Wu, J.; Guan, K.-L. TSC2 is phosphorylated and inhibited by Akt and suppresses mTOR signalling. *Nat. Cell Biol.* **2002**, *4*, 648–657. [CrossRef] [PubMed]
34. Inoki, K.; Li, Y.; Xu, T.; Guan, K.-L. Rheb GTPase is a direct target of TSC2 GAP activity and regulates mTOR signaling. *Genes Dev.* **2003**, *17*, 1829–1834. [CrossRef] [PubMed]
35. Zheng, T.; Zhou, Y.; Xu, X.; Qi, X.; Liu, J.; Pu, Y.; Zhang, S.; Gao, X.; Luo, X.; Li, M.; et al. MiR-30c-5p loss-induced PELI1 accumulation regulates cell proliferation and migration via activating PI3K/AKT pathway in papillary thyroid carcinoma. *J. Transl. Med.* **2022**, *20*, 20. [CrossRef] [PubMed]
36. Qie, S.; Diehl, J.A. Cyclin D1, cancer progression, and opportunities in cancer treatment. *J. Mol. Med.* **2016**, *94*, 1313–1326. [CrossRef] [PubMed]
37. Diehl, J.A.; Cheng, M.; Roussel, M.F.; Sherr, C.J. Glycogen synthase kinase-3beta regulates cyclin D1 proteolysis and subcellular localization. *Genes Dev.* **1998**, *12*, 3499–3511. [CrossRef] [PubMed]
38. Song, W.; Liu, Z.; Shi, C.; Wang, G.; He, L.; Chen, Z.; Li, Y.; Yu, Y.; Jiang, R.; Wang, X.; et al. RAN-S100A10-EGFR axis facilitates papillary thyroid cancer metastasis by PI3K/AKT signaling. *Cell Death Dis.* **2026**, *17*, 510. [CrossRef] [PubMed]
39. Huang, F.; Wang, H.; Xiao, J.; Shao, C.; Zhou, Y.; Cong, W.; Gong, M.; Sun, J.; Shan, L.; Hao, Z.; et al. SLC34A2 Up-regulation And SLC4A4 Down-regulation Correlates With Invasion, Metastasis, And The MAPK Signaling Pathway In Papillary Thyroid Carcinomas. *J. Cancer* **2021**, *12*, 5439–5453. [CrossRef] [PubMed]
40. Li, J.J.; Ru, Z.X.; Yang, X.; Sun, J.-X.; Wu, Y.-M.; Yang, X.-Y.; Hou, B.-Y.; Xue, B.; Ding, C.; Qiao, H. Circ_0004851 regulates the molecular mechanism of miR-296-3p/FGF11 in the influence of high iodine on PTC. *J. Transl. Med.* **2024**, *22*, 586. [CrossRef] [PubMed]
41. Clifton-Bligh, R.J. Mechanisms of resistance to RET-directed therapies. *Endocr. Relat. Cancer* **2025**, *32*, e240224. [CrossRef] [PubMed]
42. Wei, Y.; Zhang, Y.; Zhang, Z.; Wang, Y.; Li, P. Molecular pathogenesis and therapeutic advances in RET fusion-positive papillary thyroid carcinoma. *Pathol. Res. Pract.* **2026**, *281*, 156407. [CrossRef] [PubMed]
43. Rump, A.; Eder, S.; Hermann, C.; Lamkowski, A.; Kinoshita, M.; Yamamoto, T.; Take, J.; Abend, M.; Shinomiya, N.; Port, M. Modeling principles of protective thyroid blocking. *Int. J. Radiat. Biol.* **2022**, *98*, 831–842. [CrossRef] [PubMed]

Disclaimer/Publisher's Note: The statements, opinions and data contained in all publications are solely those of the individual author(s) and contributor(s) and not of MDPI and/or the editor(s). MDPI and/or the editor(s) disclaim responsibility for any injury to people or property resulting from any ideas, methods, instructions or products referred to in the content.